Bioinformatics, 31(16), 2015, 2705–2712
doi: 10.1093/bioinformatics/btv216
Advance Access Publication Date: 21 April 2015
Original Paper

OXFORD

Systems biology

Analysis of impedance-based cellular growth assays

Franziska Witzel[1,2,4], Raphaela Fritsche-Guenther[3], Nadine Lehmann[1,4], Anja Sieber[1,4] and Nils Blüthgen[1,2,4,*]

[1]Institute for Pathology, Charité Universitätsmedizin Berlin, 10117 Berlin, [2]Institute of Theoretical Biology, Humboldt-Universität zu Berlin, 10115 Berlin, [3]BIMSB, Max-Delbrück-Centrum für Molekulare Medizin, 13092 Berlin and [4]Integrative Research Institute Life Sciences, Humboldt-Universität zu Berlin, 10099 Berlin, Germany

*To whom correspondence should be addressed.
Associate Editor: Jonathan Wren

Received on December 23, 2014; revised on March 27, 2015; accepted on April 14, 2015

Abstract

Motivation: Impedance-based technologies are advancing methods for measuring proliferation of adherent cell cultures non-invasively and in real time. The analysis of the resulting data has so far been hampered by inappropriate computational methods and the lack of systematic data to evaluate the characteristics of the assay.

Results: We used a commercially available system for impedance-based growth measurement (xCELLigence) and compared the reported cell index with data from microscopy. We found that the measured signal correlates linearly with the cell number throughout the time of an experiment with sufficient accuracy in subconfluent cell cultures. The resulting growth curves for various colon cancer cells could be well described with the empirical Richards growth model, which allows for extracting quantitative parameters (such as characteristic cycle times). We found that frequently used readouts like the cell index at a specific time or the area under the growth curve cannot be used to faithfully characterize growth inhibition. We propose to calculate the average growth rate of selected time intervals to accurately estimate time-dependent IC50 values of drugs from growth curves.

Contact: nils.bluethgen@charite.de

Supplementary information: Supplementary data are available at *Bioinformatics* online.

1 Introduction

Cell proliferation assays in multiwell format have become one of the main workhorses in drug characterization and are used for cellular phenotyping (Basu *et al.*, 2013; Garnett *et al.*, 2012). Screening of thousands of compounds from drug libraries requires very cost-efficient approaches. Classical proliferation assays like the MTT or XTT assay have a number of disadvantages. They are often not very quantitative and are typically invasive, as they require labels which influence cellular metabolism. Since culturing of the cells and application of the assay is the most laborious task, typically the assay is performed only at a few time points after application of the drug. Consequently, these assays may miss important kinetic information.

Targeted therapies and *ab initio* design of novel kinase inhibitors require more quantitative evaluation of drug effects on cell phenotype. Kinase inhibitors typically have nontrivial pharmacodynamics that depends crucially on cell type and mutation pattern. Thus, it is desired to record growth curves non-invasively and with high temporal resolution. Such a method for studying cellular processes in real time was developed in the 1980s and became known as electric cell-substrate impedance sensing (ECIS) (Giaever and Keese, 1993). In this assay, the cell culture well bottom contains electrodes, typically a large reference electrode and one or several detection electrodes. Via these electrodes, a small alternating potential is applied, and the impedance of the circuit is measured. Cells that grow on the

detection electrodes increase the measured impedance, thus the impedance should correlate with the number of cells. This method has also been successfully used to study electric properties of the cell membrane, the mode of cell attachment to the ground substrate as well as cell motility (Giaever and Keese, 1991, 1993) and to analyze cytotoxicity (Xiao and Luong, 2003; Xiao *et al.*, 2002). Solly *et al.* (2004) developed an assay called real-time cell electronic sensing, which is based on ECIS; however, the electrode structure has been improved to allow detection of almost all cells in a culture well. Assay plates are now commercially available in multiwell format.

In this study, we investigated how to improve the analysis of growth curves measured by the assays. First, we compared cell index data obtained by the assay with data on % confluency from microscopy. The analysis shows that the assay can be used to study proliferation quantitatively, as the measured cell index relates linearly to the cell surface of adherent colon carcinoma cell lines. Next we evaluated if mathematical models can be used to describe the time-resolved measurements. We found that after seeding, adherent cells require a certain time to attach to the surface, after which they start to grow exponentially. The duration of the exponential growth phase depends critically on initial cell number and the culture well capacity, as increasing relative confluency will lead to contact inhibition of growth. After evaluating different growth models, we concluded that the different phases of the cell growth (after cell attachment) can be appropriately described by the Richards growth model (Richards, 1959). Parameters obtained from the model fit can be used to derive quantities that characterize cell growth, such as the doubling time of proliferating cells.

Besides, growth measurements are often used to determine quantitative traits of drugs, such as IC50 values. We found that the cell index, the normalized cell index or the area under the growth curve are error-prone readouts for quantification of growth. In contrast, growth can be quantified reliably by calculating average growth rates, and consequently these rates (when obtained from different inhibitor treatments) are suitable for IC50 estimation. Accurate time-dependent IC50 values can be obtained by sampling the average growth rate within several user-defined time intervals.

From our studies, we conclude that the technology is well suited to quantify cell growth. However, the currently applied techniques of growth curve analysis (such as the ones build into the software of commercial systems) are insufficient for extracting quantitative information. In this work, we present quantitative computational methods that make use of the dynamic information.

2 Materials and Methods

2.1 Cells and cell culture

Human colorectal cancer cell lines HCT116, RKO and HT29 were obtained from ATCC (American Type Culture Collection, UK). LIM1215 were kindly provided by Prof. John Mariadason (Ludwig Institute for Cancer Research Austin Hospital, Melbourne, Australia). HCT116, RKO and Lim1215 were maintained in DMEM (Dulbecco's Modified Eagle's Medium, Lonza), supplemented with 10% fetal calf serum, 1% ultraglutamine and 1% penicillin/streptomycin. HT29 were maintained in L-15 (Leibovitz) supplemented with 0.1% (w/v) $NaHCO_3$, 4% (w/v) glucose, 0.2% of 1.4 mg/ml insulin, 1% of 10 mM MEM vitamins (Biochrom AG), 0.5% of fetuin/transferrin solution (0.12%/0.05%) (w/v), 10% fetal calf serum, 0.5% ultraglutamine and 1% penicillin/streptomycin. All cells were incubated in a humidified atmosphere of 5% CO_2 in air at 37°C.

2.2 Reagents

The following inhibitors were used in the growth assays: Mek inhibitor U0126 (Promega), Raf inhibitor Sorafenib (LC Laboratories), PI3K inhibitor LY294002 (Axxora Deutschland) and the EGFR inhibitor Erbitux (Charité Universitätsmedizin Berlin). The solvent control was DMSO (used in the same concentration as in solutions that contain an inhibitor).

2.3 Growth measurement

Real-time analysis of proliferation was performed using the xCELLigence system RTCA SP from ACEA Biosciences. Cells are grown in the disposable E-Plate 96, a microtiter plate with gold electrode structures of biocompatible surface at the bottom of each well. Electrode and respective counter electrode have a complex interdigitated structure (as shown in Fig. 1A) and both combined cover 80% of the ground. The RTCA device measures the impedance at an alternating voltage of 20 mV and 10 kHz frequency. As the whole device is housed inside of an incubator, the cells are kept at optimal culture conditions (5% CO_2, 37°C) during the measurement. The growth assay was performed according to the instructions of the manufacturer.

2.4 Image analysis

To observe cells in the xCELLigence system, we used the E-Plate VIEW 96, where four rows of electrode structures have been left out, yielding an electrode surface coverage of 70%. Bright field images of the cells were segmented automatically using functions of the Image Processing Toolbox of MATLAB. Briefly, the gold electrode structures, which appear as well-defined dark objects in the pictures, were detected by k-means clustering of the luminosity layer and removed from the images thereafter. Cells were detected using texture segmentation, i.e. by applying a range filter that amplifies intensity variations in the neighborhood of an image pixel. We calculate confluency by counting total image pixels and pixels that make up the segmented areas.

2.5 IC50 estimation

We compare four different readouts for quantification of cell growth. These readouts are the cell index ci, the normalized cell index $ci/ci(t_{ref})$, the area under the curve and the average growth rate $\log [ci/ci(t_{ref})]$, where t_{ref} refers to a reference time point. We normalized the quantities to the respective value of the control curve (to obtain the relative inhibition Inh_{rel}) and fitted the correlation with the inhibitor concentration c to the Hill-slope model

$$Inh_{rel} = a + \frac{1-a}{1+\frac{c}{IC50}^{n}} \quad (1)$$

to obtain the parameters a (maximal relative inhibition), the steepness n and the IC50 value, using the lsqnonlin fitting routine of MATLAB.

3 Results

3.1 Impedance measurement as a non-invasive method to study proliferation of adherent cells

We first set out to investigate how well impedance measurements reflect the cell number of adherent cells. For this, we used a commercially available system (xCELLigence) (Ke *et al.*, 2011). Essentially, the instrument measures the impedance in a 96-well format. The system calculates a so-called cell index, which is proportional to the

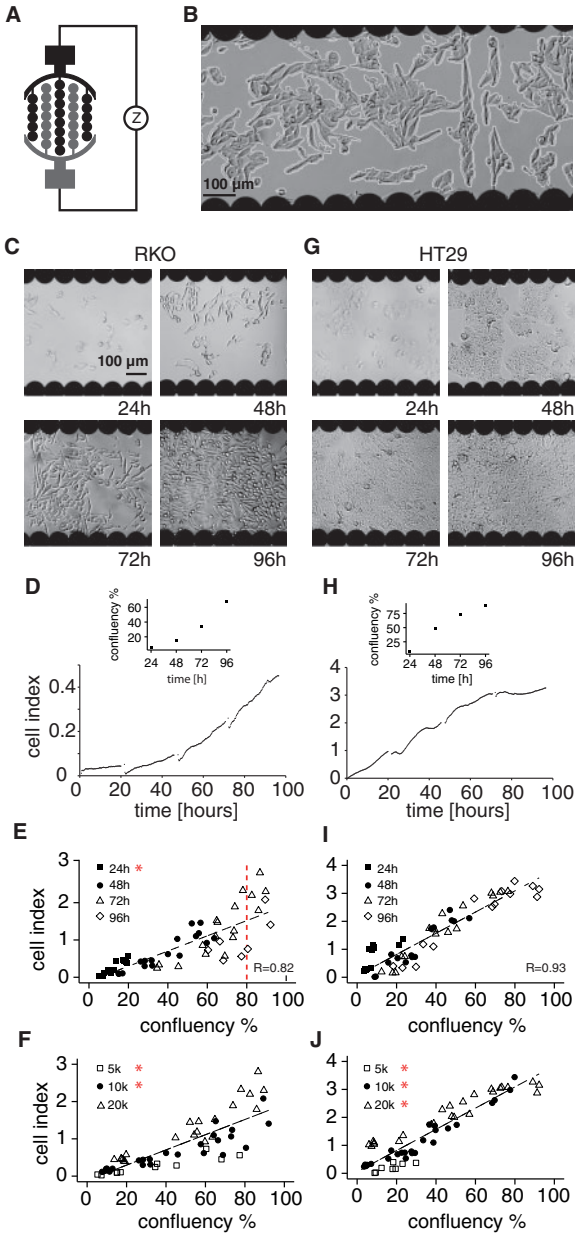

Fig. 1. Cell index correlates with cell surface and reflects proliferation. (**A**) Sketch of the electrode structures at the bottom of an E-Plate 96 well. An electrode is characterized by a circle-on-line structure, where the arrays of one electrode (shown in black) are interdigitated with the arrays of the counter electrode (shown in gray). (**B**) Automatic image segmentation is used to find the borders of cells (indicated with white lines) that are growing in the electrode structure free zone of the E-Plate VIEW 96. Analysis of correlation of cell index and % confluency of RKO cells in (**C–F**) and of HT29 in (**G–J**). Microscopic images showing proliferation (C,G) which correlates with increasing cell index values in the corresponding growth curves in panels (**D**) and (**H**). The curves are broken at times when the plate was removed for microscopic analysis. The corresponding % confluency estimated from the microscopic images is shown in the insets. The correlation of % confluency (as estimated by automated image segmentation) and measured cell index from 20 growth curves at four time points for each cell line, RKO and HT29, respectively, is resolved by the time point of analysis in panels (**E**) and (**I**) and by the number of seeded cells in panels (F) and (J) (5k cells = 5000 cells). The Pearson correlation of all data is indicated with R. A significantly improved linear correlation of a subgroup of the data is indicated with $*$ in the figure legends. The dashed line in panel (E) indicates that data with relative confluency $\leq$80% also show improved linearity. For the statistical analysis of significance, refer to the Supplementary Section 1.2

impedance from which the background (i.e. impedance of the circuit in presence of medium but without cells) is subtracted. This index increases when the electrode structures become successively covered with adherent cells. Thus, the cell index is not a direct function of cell number, but rather of the collective cell surface, the mode of cell attachment and cell membrane composition. Therefore, it is important to establish that the increase in the cell index is primarily due to the formation of new adherent cells.

To experimentally determine if the cell index faithfully reports cell numbers, we used 96-well plates in which the central four rows of the electrode structures in each well were left out, allowing to inspect relative confluency using microscopy. In these plates, we seeded either 5×10^3, 10^4 or 2×10^4 cells per well, which we either left untreated (triplicates per cell line, HT29 and RKO) or treated with Mek-inhibitor U0126 or its vehicle control DMSO (both in duplicates per cell line for cells seeded at 10^4 or 2×10^4 cells). Growth curves were recorded over a time period of 4 days with daily interruptions for microscopic analysis to estimate % confluency.

Figure 1C and G shows examples of bright field images taken from the electrode-free zone for untreated RKO (5×10^3 cells/well initially) and HT29 (2×10^4 cells/well initially) at the indicated time points. The corresponding growth curves are shown in Figure 1D and H. To determine the relative confluency in an unbiased way, we used automated image segmentation to find the borders of cells (as shown in Fig. 1B) and counted the image pixels covered by cells. The insets of Figure 1D and H show the % confluency that was estimated for RKO and HT29 cells from images in Figure 1C and G. In independent experiments where we used life-cell imaging with nuclear markers, we established that the cell surface area is linearly correlated with cell number for these cells (see Supplementary Figs S1 and S2).

Next we related the relative confluency with the cell index. Figure 1E,F and I,J show the results for RKO and HT29, respectively. There is a clear linear correlation of % confluency with cell index for the cell line HT29 with a Pearson correlation coefficient of 0.93. For very high relative confluency (close to 100%), the curve shows saturation. The reason for this is unclear. Estimation errors may arise as we extrapolate cell % confluency of the whole well from the small proportion of the well that is accessible for microscopy. Also, in a previous study, it was found that in general, the cell index represents cell number only for sub-confluent cultures (Solly *et al.*, 2004). In line with this, we often observed significant changes in the cell index even after the cells have reached confluency, which might reflect changes in the cells mode of attachment. Consequently, impedance growth curves should not be evaluated as proportional to cell number after the curve has approached a plateau.

For RKO cells, we observed stronger deviations from linearity, the Pearson correlation was 0.82 when all data points are taken into account. Again, deviation resulted mainly from data at high % confluency, and linear correlation was significantly higher when only data below a level of 80% confluency were taken into account (indicated with the dashed line in Fig. 1).

Visual inspection of the data shown in Figure 1F and J suggested that correlation within the groups of cells seeded at the same density is higher than overall correlation. The cell index seems to have shifted to higher values in a systematic fashion with increasing numbers of seeded cells (subgroups with significantly improved correlation are marked with a star in Figure 1E, F, I and J, see Supplementary Section 1.2 for the statistical analysis). One interpretation is that initial cell density influences the attachment mode and thus also subsequent measurements of the cell index. These

results suggest that generally assays should be started with the same number of seeded cells to make them comparable.

Another parameter that could influence linearity is a change of the properties of the growth medium over time. The measured impedance could be influenced by changes in temperature and pH of the medium, which is acidified over time by the cellular metabolism. Grouping the data by the time point of measurement, however, did not lead to significant improvement in the linear correlation, except for the 24 h subgroup of RKO cell data (Fig. 1E and I). Data of later time points for RKO are rather characterized by a higher spread which might be due to almost total confluency. However, there are some more indications for an influence of the growth medium. For instance, the impedance measured after each microscopic analysis is reduced compared with the impedance measured before the plate was removed (see growth curve of RKO cells in Fig. 1D). RKO cells have been cultured in DMEM which has a bicarbonate buffer system and thus heavily depends on the ambient CO_2 concentration. When wells that contained only medium were measured, the cell index dropped constantly, both for DMEM and L-15 (see Supplementary Fig. S3). Assuming that this effect contributes in a linear fashion to the cell index, this would increase inaccuracies for later time points of the measurement. We have reevaluated the correlation of % confluency with cell index after subtraction of medium curves and found only slight improvements in linearity of % confluency and cell index (Supplementary Fig. S3). However, it is beyond our scope to estimate in which way the medium impedance contributes to the total measured impedance. Medium changes during time-course experiments should be avoided as they perturb the correlation between cell index and cell number. We conclude that the cell index reports % confluency of RKO and HT29 cells with acceptable accuracy, as long as the culture is sub-confluent and the experimenter seeds the same amount of cells in each well. The % confluency also relates to cell number, as long as the cells are far from confluency where their contact surface might be significantly decreased.

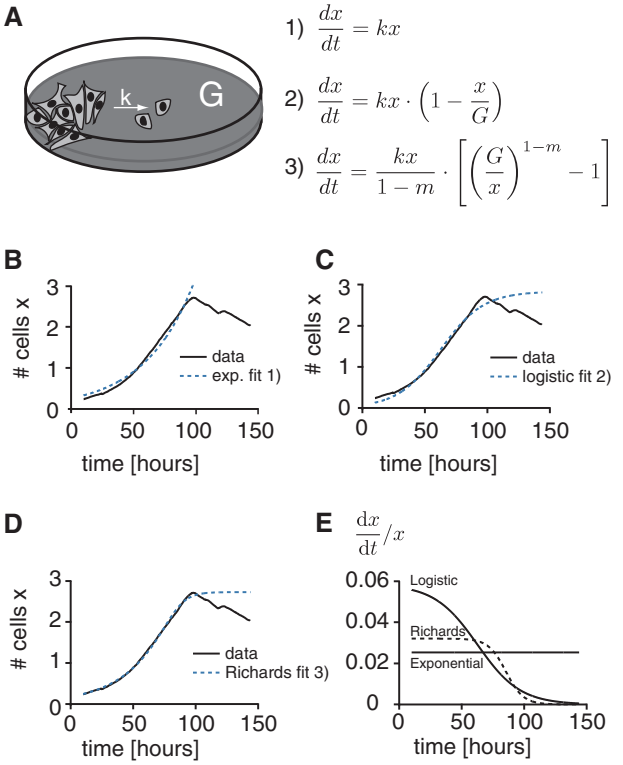

Fig. 2. Model selection. (**A**) The growth of adherent cells in confined space. The growth rate constant *k* is determined by the speed of cell division. The maximum cell index *G* is mainly the result of a limited surface for adherent cell growth of a cell monolayer. The exponential (1) and the logistic growth model (2), as well as the growth model according to Richards (3) are presented in their differential form. (**B–D**) The integrated form of the three different growth models (for integrated forms see Supplementary Table S4) was fitted to the growth curve of RKO cells, which were seeded at a density of 100 cells/μl and left untreated. We draw in panel (**E**) how the relative growth rate (h^{-1}) changes over time as predicted from the three different model fits

3.2 Model-based analysis of growth curves

After having established that the cell index can be used as a linear measure of cell number, we next aimed to describe the growth curves using mathematical models. This offers the possibility to reliably estimate various factors like the cells' characteristic growth rate, contact inhibition and kinetics of drug action. We investigated three models to describe cell growth with increasing model complexity. The simplest reasonable growth model is exponential growth, which is the solution of a linear ordinary differential equation (ODE) where growth is proportional to the cell number and the growth rate *k* (ODE 1 in Fig. 2A). The second model has an additional parameter *G* that reflects the maximal capacity of the well, and the growth rate decreases with cell number until *G* is reached (ODE 2 in Fig. 2A). This model is known as the Logistic equation (Verhulst, 1845) and was used to predict the population dynamics of countries and has since then been successfully used in theoretical ecology. The third model is a generalization of the logistic growth model, the so-called Richards model (Richards, 1959) (ODE 3 in Fig. 2A). In this model, an additional 'shape' parameter *m* changes the sharpness in which growth rate is reduced. For $m = 2$, the Richards model coincides with the Logistic model, and with increasing *m*, the transition to lower growth rates is shifted to later time points. None of the three models can describe the initial process of cell attachment, and to compare the performance of the models independent of this deficit, we omitted the data from the first 10 h. Practically, however, parameter estimation is not influenced by the omitted time interval and even performs similarly well if the whole growth curve is used for fitting (see Supplementary Fig. S4).

When fitting these three models to the experimental data, we observed that both the simple exponential growth model and the logistic equation do not faithfully describe the kinetics (see Fig. 2B and C, respectively). In contrast, the Richards model fits the growth curve with high quantitative accuracy (Fig. 2D). Figure 2E shows schematically for these three models, how the growth rate $\frac{dx}{dt}/x$ changes over time. In the exponential model, the growth rate is constant, whereas the growth rate is steadily decreasing in the logistic model. In contrast, the Richards model (for $m > 2$) has an extended period with constant growth rate, which is followed by a rather fast decline, similarly to what is seen in real growth rates. Accordingly, the Richards model fits the first 100 h of the growth curve very well (Fig. 2D), from which we can draw the conclusion that in this example the cells grow exponentially (with a constant rate) during the first ≈60 h, before contact inhibition starts to reduce growth. After about 100 h, the growth curve drops, which might be attributed to advancing medium acidification, cell death due to consumption of nutrients or detaching cells. The model presented here was not intended to capture these processes, and thus data points at these late time points need to be removed from the analysis. Although simpler models systematically deviate from the growth curves, the Richards model describes the data with reasonable accuracy.

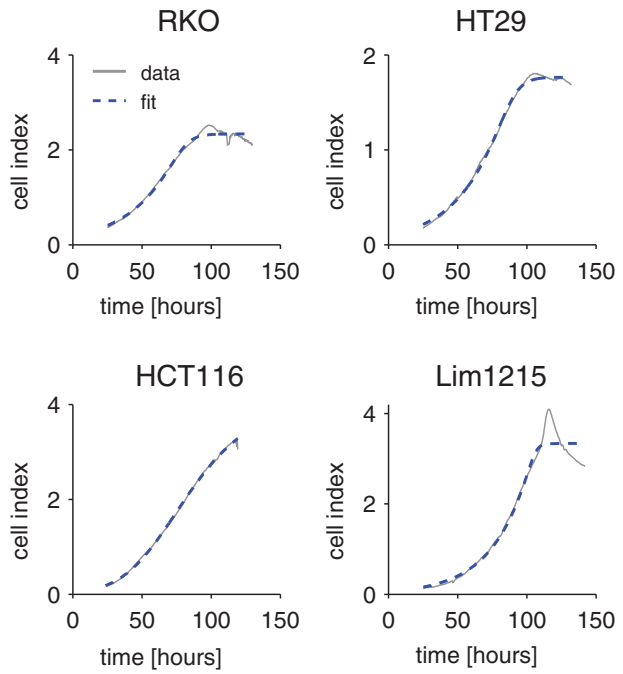

Fig. 3. Richards model fit. The Richards model can be used to fit the growth curves of different sub-confluent colon cancer cell lines. The figure shows one exemplary growth curve and the respective fit of the Richards model for each cell line. Parameters of the fit are shown in the Supplementary Table S5 in the Supplementary Material

Most importantly, it is the only model that can describe the biphasic growth processes observed in all tested cell lines where an extended exponential growth phase is followed by a rather short phase of saturation (Fig. 2E). Also, the additional shape parameter makes the Richards model much more flexible and applicable in a general fashion than the logistic model.

From the parameters of the fitted Richards model, one can calculate the characteristic cell cycle time, by the following equation:

$$t_2 = \frac{m-1}{k} \ln 2 \qquad (2)$$

This formula is based on the growth rate for small cell numbers and thus represents a lower limit of the cell cycle time with zero contact inhibition. We used fits of the Richards model to datasets of four different colon cancer cell lines to obtain estimates for the doubling time. Figure 3 shows representative model fits and Table 1 contains the estimated doubling times. Interestingly, they range from just below 10 h (HCT116 cells) to 22 h (HT29 cells). The variability of the growth curves within an experiment is less pronounced than between different experiments (see Supplementary Fig. S5 for all growth curves the analysis is based on). The surprisingly short doubling time of about 10 h in HCT116 cells is not an artifact of the Richards model fitting procedure and can be confirmed when fitting an exponential model to the period of the assay where the cells grow with constant rate (Supplementary Fig. S6). We additionally estimated the cycle time from a live cell imaging experiment and obtained $t_2 = 10.7 \pm 1.9$ h, which compares with the impedance-based result (details in Supplementary Fig. S7).

The Richards model is a flexible growth model for cells that grow with a constant growth rate under the influence of contact inhibition. However, different phenomena like time-dependent inhibition or cell cycle synchronization of the cells might create more complicated growth curves (e.g. see Supplementary Fig. S8). Constructing a model of higher complexity to account for that is feasible; however, parameterization can become difficult. In the next section, we outline how complex time-dependent inhibition profiles can be evaluated without model fitting.

Table 1. Cell cycle times of colon cancer cell lines

RKO	HT29	HCT116	Lim1215
20.8 ± 0.6 h	22.2 ± 2 h	9.6 ± 2.6 h	21.1 ± 3.9 h

Cycle times have been determined from the parameters of 12 independent model fits (12 technical replicates for RKO and 12 replicates from 4 experiments for the other cell lines) according to formula (2). The respective growth curves are shown in Supplementary Figure S5

3.3 Using growth curves to characterize the effect of small-molecule inhibitors

Next we asked how the growth curves can be used to extract information about the action of small molecule inhibitors. As an example, we investigate how the inhibitor concentration of half maximal inhibition, best known as the IC50 value, can be most reliably calculated from the growth curves. Often, the inhibitor affects cell growth in a complex time-dependent manner, thus a model-based analysis would depend crucially on the assumption about the time profile of the inhibitor. Here we concentrate on estimating the average effect of an inhibitor in a time interval, which is a typical question in pharmacology. To benchmark different approaches, we used datasets generated *in silico* using the Richards growth model, in which we modeled the effect of the inhibitor by decreasing the growth rate k according to the Hill-slope model [Equation (1), see also (Sebaugh, 2011)] with half-maximal inhibition at IC50 = 4 μM (Fig. 4A).

Figure 4B shows the simulated growth curves for the set of growth rates from Figure 4A. All curves start with the same initial cell number or cell index. However, in experiments, the initial cell index from different wells is subject to variations due to the pipetting error and differences in the number of cells that actually survive and attach after seeding. As the initial phase of cell growth (after cell attachment) is exponential, the error becomes more pronounced after a few hours of growth. Typically, the cells are incubated for 24 h prior to inhibitor application, so that the spread in cell index values amplifies during this period of time. Increased initial cell number may lead to an apparent increase in growth rate, as the absolute increase of the cell index is larger for higher number of cells. Figure 4C shows the influence of varying initial cell numbers. Here, three growth curves have been calculated for a high growth rate (representing control cells) and a low growth rate (representing inhibited cells), which differ by the initial cell index. One of the growth curves with low k (upper dashed line) has a slightly higher initial cell number, and it seems that growth is faster than in the other two growth curves with the same k (other two dashed lines). It shows that the cell index value at a given time point alone does not help to reliably estimate growth.

To investigate how well different methods of IC50 estimation perform in a realistic setting, we have generated 10 000 sets of growth curves for six inhibitor concentrations with initial cell indices placed randomly between 0.2 and 0.4, reflecting the experimentally observed spread of cell index at 24 h after seeding. For all 10 000 sets, we have estimated the IC50 at 24, 48 and 72 h after inhibitor application, with four different methods: (i) the ci value at a given time point, (ii) the area under the curve up to the time point,

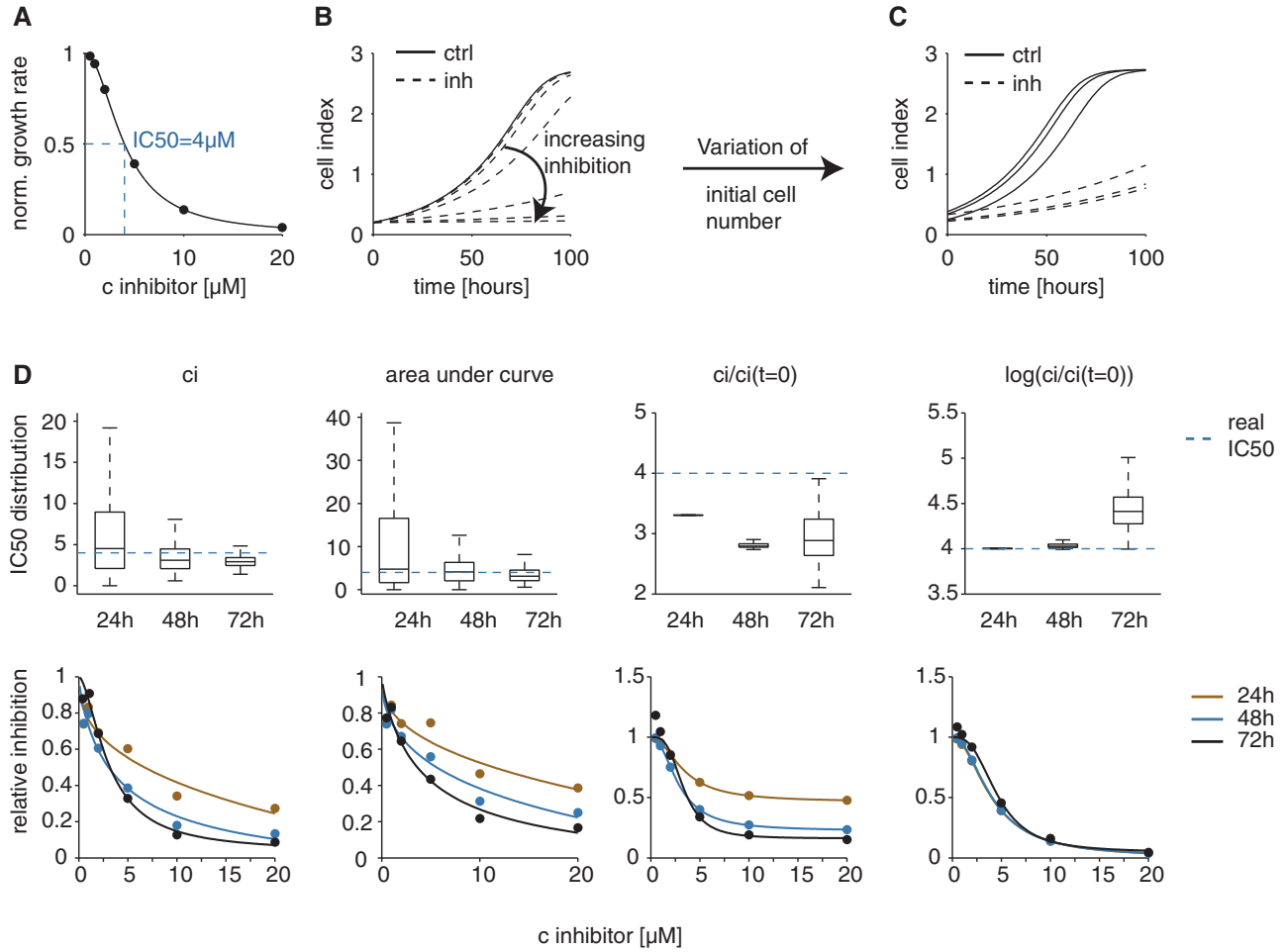

Fig. 4. The estimation of the IC50 value from growth curves. We use the model of Richards to simulate growth curves with increasing degree of inhibition, by reducing the growth rate *k* while all other parameters are left unchanged. The various growth rates are related to different concentrations of the inhibitor according to the Hill-slope model with IC50 of 4 μM (**A**). The *in silico* growth curves resulting from the different growth rates from (A) are shown in (**B**). Slight variation of the initial cell index mimics inhibition, which is illustrated in panel (**C**). We show theoretical triplicates of either a control growth curve (solid line) or a treated growth curve (dashed line), respectively, where all parameters are identical, except for the initial cell index at $t=0$. Panel (**D**) shows how different ways of IC50 calculation perform, when we analyze growth curves with continuously decreasing growth rate as shown in panel (B); however, the initial cell index is randomly varied on a cell index interval of [0.2,0.4]. The upper row shows the distribution of estimated IC50s from 10 000 trials, when they were either determined after 24 h, 48 h or 72 h (outliers of the distribution were omitted in this figure). The fit of relative inhibition versus inhibitor concentration [using Equation (1)] that leads to the respective IC50 value is shown exemplary for one trial in the lower panel. The four different methods of IC50 calculation are described in the main text

(iii) the normalized ci value ci(t)/ci($t=0$) of the time interval and (iv) the logarithm of the normalized ci value for the time interval. The distribution of the estimated IC50 values is shown in the upper panels of Figure 4D. The lower panels of the figure show one exemplary fit (out of 10 000) of the respective quantity (normalized to the solvent control) versus concentration of the inhibitor using the Hill-slope model Equation (1). The methods can be compared based on two criteria: first, the ability of the method to identify the right IC50 of 4 μM and, second, the robustness of the estimator.

The simplest method is to calculate the IC50 from the cell index value that is reached at a specific time, e.g. at 24 h. When applying this method to the simulated data, resulting IC50 value estimations varied strongly, spreading on an interval between close to 0 and 18 μM, and 50% being more than a factor of two away from the real IC50 at 4μM (see left upper panel in Fig. 4D). After 48 h and even more so after 72 h, the influence of the initial cell index spread on the estimated IC50 is reduced; however, the median of the estimations deviates to lower IC50 values. Thus, this method biases the estimate of the IC50 value. Another frequently used approach is to calculate the IC50 based on the area under the growth curve (upper panel, 2nd from left, Fig. 4D). As the area is proportional to the arithmetic mean of the cell index, it is not surprising that it is also a non-robust estimator with similar bias. Obviously, both methods suffer from the influence of the initial cell index. Not surprisingly, normalizing the cell index by the initial cell index reduces the spread of the estimation (see upper panel, 2nd from right, Fig. 4D). However, this estimator systematically underestimates the IC50. This is primarily because the ratio of cells at different time points is not proportional to the growth rate. Thus, we reasoned that for near-exponential growth, the number of cell doublings within a time window is the better measure. This quantity can be calculated by taking the logarithm to the base 2 of the normalized cell index, as shown in the upper right panel of Fig. 4D. Using this estimate, the correct IC50 can be found independently of the initial cell index, with very little uncertainty and no bias at early time points. The logarithm of the normalized cell index is in accordance with an average growth rate, per definition. Consequently, this measure can be used to reliably calculate IC50 values, over a time interval, in which

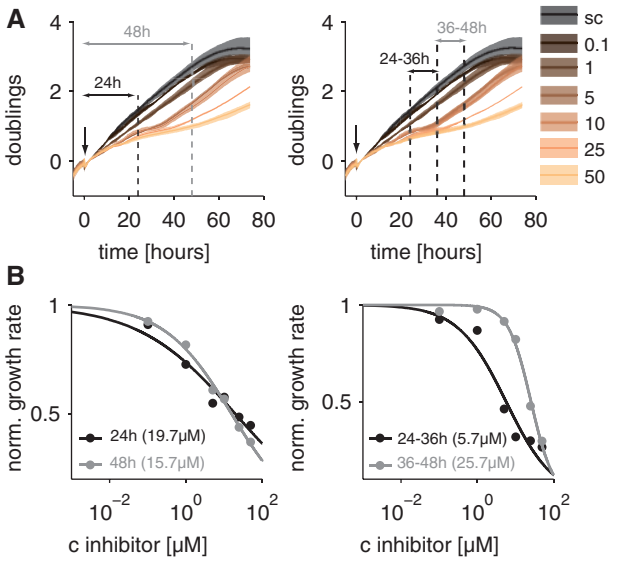

Fig. 5. Time-dependent IC50 of U0126 in HT29 cells. HT29 cells have been treated with various concentrations of U0126 (concentrations in legend in μM) ca. 20 h after seeding and sc is the solvent control DMSO. In (**A**), the solid lines show the mean number of doublings since inhibitor application from three replicates. The spread around the lines reaches from the minimum to the maximum value of the replicates. The IC50 value of U0126 has been estimated over an interval of 24 h and 48 h after inhibitor application (left panel in A) and over the time interval between 24 and 36 h or 36 and 48 h (right panel in A). The corresponding fits of the Hill-slope model (1) with $a=0$ are shown in panel (**B**). The legend indicates the time interval from which the data have been taken and the respective estimated IC50 value in parentheses

the cells still grow exponentially. However, if the average growth rate is calculated at 72 h, some cells are already contact inhibited and grow slower not because of the inhibitor but due to this spatial limitation. As a consequence, the growth rate of cells treated with lower inhibitor concentrations approaches the growth rate of cells treated with higher concentrations which are not contact inhibited and it seems like the inhibitor is less effective, hence the IC50 value becomes slightly overestimated (Fig. 4D upper right panel, at 72h). We conclude that by using the average growth rate (or number of cell doublings), the IC50 can be well estimated, without bias and with little influence of initial spread of the cell index. The experimenter can choose the time interval *ad libitum* (e.g. the average growth rate between 28 and 42 h). Thus, a time-dependent IC50 value can be generated by sampling different time intervals of the growth curve. In this way, inhibitor kinetics may be revealed, even when the time-dependent growth rate $k(t)$ is not directly accessible. Later time points of the growth assay cannot be analyzed, as contact inhibition obscures the effect of a proliferation inhibitor.

Finally, we illustrate the average growth rate approach for IC50 estimation on the basis of a dataset of HT29 cells, which had been treated with different concentrations of U0126 (triplicates per treatment). In Figure 5A, we show the growth curves in a transformed version, as doubling events since 2 h after inhibitor application (our reference time t_{ref}). All cell index values (ci) of the curve are transformed according to

$$\text{doublings} = \log_2 \frac{\mathrm{ci}(t)}{\mathrm{ci}(t_{\mathrm{ref}})}. \qquad (3)$$

There are two advantages of this transformation. First, it enables averaging over replicates. In this figure, each solid line represents the mean of three replicates and the shade spreads from the minimum to the maximum value of the replicates. The spread of the data is greatly reduced compared with the presentation of raw cell index values, which are influenced by the initial value (see Supplementary Fig. S9 for a plot of the raw data). Second, the slope in these curves is proportional to the growth rate. By comparing the slopes, it can be said already by eye inspection, which cells grow faster than others. In this experiment, we see time-dependent inhibition. Between 24 and 36 h, cells that were treated with more than 10 μM of U0126 are basically growth arrested (see right panel of Fig. 5A), whereas growth restarts in the next 12 h. Accordingly, the IC50 value calculated based on the average growth rate between 24 and 36 h is almost 5-fold lower than the derived IC50 value based on the next 12 h (see right panel of Fig. 5B). This effect is much less pronounced when the IC50 value is derived based on the average growth rate of the first 24 h or 48 h after inhibitor application (left panels of Fig. 5A and B).

This example shows that growth curves offer a wealth of information when it comes to the time-dependent effects of inhibitors and that the time window chosen for analysis will influence what properties can be extracted. Time intervals in which some treatment leads to growth arrest are of general interest when characterizing inhibition kinetics.

4 Discussion and Conclusion

Use of impedance-based technologies to monitor various different types of cells over time has become more popular in the last years, and about 30% of recorded publications at Pubmed (search terms xCELLigence AND proliferation) have been published in 2014. These reports include proliferation studies on human cancer cell lines (Caputo *et al.*, 2014; Dowling *et al.*, 2014; Módis *et al.*, 2014); however, the authors mostly restrict the data analysis to rather qualitative descriptions.

The analysis of proliferation with the xCELLigence technology crucially depends on the linear correlation of the cell index to the cell number. Linearity has been shown for the cell index from BALB/c 3T3 (Xing *et al.*, 2006) and NIH 3T3 cells (Xing *et al.*, 2005) when they were seeded at different densities and measured 6 h thereafter. We have exemplarily shown that the cell index faithfully reports cell-covered area throughout the time course of 4 days, by comparing the cell index with the total cell surface estimated by microscopy.

We have found that the Richards growth model appropriately describes the growth curves of various colon cancer cell lines in the xCELLigence system. In this model, exponential growth eventually slows down most likely due to contact inhibition. However, the model formulation is empirical—geometrical aspects of two dimensional cell growth are ignored. In the extreme case where all cells are seeded in one spot, contact inhibition takes effect immediately and virtually only the cells at the border of the colony will still proliferate. The consequence would be a quadratic growth law instead of the expected exponential growth (Cherry and Papoutsakis, 1989). However, the ability of cells to migrate might counteract the limitation of proliferation to cells at the border. The concerted effects of cell seeding patterns and cellular migration on proliferation have been studied with a cellular automaton model (Lee *et al.*, 1995). Surprisingly, at uniform distribution of cells in the culture well, the stochastic simulation produces growth curves that show strong similarity to the Richards growth model. As HT29 and RKO cells are characterized by rather low basic migration rates, we conclude that the even distribution of cells after seeding is the main reason for the observed initial period of

exponential growth, where contact inhibition severely affects the growth kinetics only close to confluency. This explains why the empirical and thus rather simple Richards model is perfectly suited for our intentions. Because of its flexibility concerning the time course of growth inhibition, it has been used widely to describe growth curves (Tjørve and Tjørve, 2010). By fitting the model to the data, one can determine the doubling times during the exponential growth phase at total absence of contact inhibition.

Currently, one of the major usages of this technology is to compare growth under different conditions. For example, growth measurements using different concentrations of inhibitors are used to estimate the IC50 value. However, we show that currently applied techniques to extract quantitative parameters from the growth curves are unreliable. Neither the area under the curve nor the slope of a growth curve corresponds to the average growth rate. Though the calculation of a normalized cell index creates robustness toward fluctuations of the initial cell number, it is frequently and wrongly believed that this parameter presents a proper measure of the growth rate. We have shown that the logarithm of the normalized cell index corresponds to the average growth rate of a time interval and this measure also compensates for fluctuations of the initial cell index. As a consequence, we do not recommend averaging over the raw cell index values of replicates but to average the logarithm of the normalized cell index.

Average growth rates, over time intervals of *ad libitum* choice, are suited for calculation of time dependent IC50 values. The commercial software that is shipped with the instrument (RTCA software, version 2.0 January 2013) offers the possibility to use either the raw cell index values, the normalized cell index values or the area under the curve for IC50 analysis—yet none of these quantities represent the degree of inhibition in terms of the effect on the cells growth rate, rendering the RTCA software insufficient for analysis of proliferation. Also in cytotoxicity assays, the logarithmic transformation of the data can be beneficial for IC50 determination as apoptosis reflects an exponential decay of the cell index. The calculation of average growth rates is not recommended for migration or invasion assays as these processes may not follow exponential kinetics.

Compared with conventional label-based proliferation assays, impedance-based assays offer kinetic information while saving working time. Experimental errors are reduced greatly, as the various time points are obtained from one and the same well, and small pipetting errors between different wells can be compensated for by evaluating average growth rates. On the other hand, the cell impedance is a complex quantity which depends on different cell parameters. It has been observed that a decrease in cell index is not always associated with cytotoxicity, just like an increased cell index does not have to reflect proliferation (Atienzar *et al.*, 2011). Thus, we believe it remains essential to verify whether the measured increase of the cell index faithfully represents proliferation. Given this condition is fulfilled, we have shown how model fitting or the calculation of average growth rates of defined time intervals can be used to really benefit from the valuable kinetic information that impedance-based proliferation assays provide.

Funding

This work was supported by the German Federal Ministry of Education and Research through grants FORSYS and OncoPath.

Conflict of Interest: none declared.

References

Atienzar,F.A. *et al.* (2011) The use of real-time cell analyzer technology in drug discovery: defining optimal cell culture conditions and assay reproducibility with different adherent cellular models. *J. Biomol. Screen.,* **16**, 575–587.

Basu,A. *et al.* (2013) An interactive resource to identify cancer genetic and lineage dependencies targeted by small molecules. *Cell,* **154**, 1151–1161.

Caputo,E. *et al.* (2014) Aurka inhibitors enhance the effects of b-raf and mek inhibitors in melanoma treatment. *J. Transl. Med.,* **12**, 216.

Cherry,R.S. and Papoutsakis, E.T. (1989) Modeling of contact-inhibited animal cell growth on flat surfaces and spheres. *Biotechnol. Bioeng.,* **33**, 300–305.

Dowling,C.M. *et al.* (2014) Using real-time impedance-based assays to monitor the effects of fibroblast-derived media on the adhesion, proliferation, migration and invasion of colon cancer cells. *Biosci. Rep.,* **34**, e00126.

Garnett,M.J. *et al.* (2012) Systematic identification of genomic markers of drug sensitivity in cancer cells. *Nature,* **483**, 570–575.

Giaever,I. and Keese,C.R. (1991) Micromotion of mammalian cells measured electrically. *Proc. Natl. Acad. Sci. U S A,* **88**, 7896–7900.

Giaever,I. and Keese,C.R. (1993) A morphological biosensor for mammalian cells. *Nature,* **366**, 591–592.

Ke,N. *et al.* (2011) The xcelligence system for real-time and label-free monitoring of cell viability. *Methods Mol. Biol.,* **740**, 33–43.

Lee,Y. *et al.* (1995) A cellular automaton model for the proliferation of migrating contact-inhibited cells. *Biophys. J.,* **69**, 1284–1298.

Módis,K. *et al.* (2014) Effect of s-adenosyl-l-methionine (sam), an allosteric activator of cystathionine–synthase (cbs) on colorectal cancer cell proliferation and bioenergetics in vitro. *Nitric Oxide,* **41**, 146–156.

Richards,F.J. (1959) A flexible growth function for empirical use. *J. Exp. Bot.,* **10**, 290–301.

Sebaugh,J.L. (2011) Guidelines for accurate ec50/ic50 estimation. *Pharm. Stat.,* **10**, 128–134.

Solly,K. *et al.* (2004) Application of real-time cell electronic sensing (rt-ces) technology to cell-based assays. *Assay Drug Dev. Technol.,* **2**, 363–372.

Tjørve,E. and Tjørve,K.M.C. (2010) A unified approach to the Richards-model family for use in growth analyses: why we need only two model forms. *J. Theor. Biol.,* **267**, 417–425.

Verhulst,P.F. (1845) Recherches mathématiques sur la loi d'accroissement de la population. *Nouveaux mémoires de l'Académie Royale des Sciences et Belles-Lettres de Bruxelles,* **18**, 14–54.

Xiao,C. and Luong,J.H.T. (2003) On-line monitoring of cell growth and cytotoxicity using electric cell-substrate impedance sensing (ecis). *Biotechnol. Prog.,* **19**, 1000–1005.

Xiao,C. *et al.* (2002) Assessment of cytotoxicity using electric cell-substrate impedance sensing: concentration and time response function approach. *Anal. Chem.,* **74**, 5748–5753.

Xing,J.Z. *et al.* (2005) Dynamic monitoring of cytotoxicity on microelectronic sensors. *Chem. Res. Toxicol.,* **18**, 154–161.

Xing,J.Z. *et al.* (2006) Microelectronic cell sensor assay for detection of cytotoxicity and prediction of acute toxicity. *Toxicol. in vitro,* **20**, 995–1004.